Scientific Journals
of the Maritime University of Szczecin

Zeszyty Naukowe
Akademii Morskiej w Szczecinie

2020, 61 (133), 9–16
ISSN 1733-8670 (Printed)
ISSN 2392-0378 (Online)
DOI: 10.17402/394

Received: 19.09.2019
Accepted: 25.02.2020
Published: 25.03.2020

Compensation of supply current harmonics, reactive power, and unbalanced load current balance in the closed-loop control of a shunt active power filter

Agata Bielecka[1]✉, Daniel Wojciechowski[2]

[1] Gdynia Maritime University, Faculty of Electrical Engineering, Department of Ship Automation
81-87 Morska St., 81-225 Gdynia, Poland, e-mail: a.bielecka@we.umg.edu.pl
[2] Gdansk University of Technology, Faculty of Electrical and Control Engineering
Department of Electrical Engineering, Control Systems and Informatics
11/12 G. Narutowicza St., 80-233 Gdańsk, Poland, e-mail: d.wojciechowski@pg.edu.pl
✉ corresponding author

Key words: shunt active power filter (SAPF), harmonic compensation, reactive power compensation, prediction, closed-loop, open-loop

Abstract
This paper presents the compensation tasks performed by a shunt active power filter, including compensation of harmonic currents, reactive power, and an unbalanced load current. The paper demonstrates novel control of the shunt active power filter in a closed-loop system. The control algorithm was verified by performing simulations and compared the simulated results with those obtained in an open-loop control system. All simulations were conducted in the PLECS program using a control algorithm written in C programming language.

Introduction

Shunt active power filters (SAPFs) are powerful and high-quality tools to solve power quality problems. They operate as controlled current sources that inject the harmonic components generated by a nonlinear load. As a result, the components of the harmonic currents contained in the load current are cancelled by the effect of an active power filter, and the source current (and consequently the source voltage) remains sinusoidal. Moreover, with an appropriate control algorithm, SAPFs can compensate for the load power factor and unbalanced load currents. Due to this, they have become increasingly popular, and many different solutions and control strategies can be found in the literature (Mattavelli, 2001; Mariethoz & Rufer, 2002; Mattavelli & Marafão, 2004; Asiminoaeiand et al., 2006; Wojciechowski, 2012; Mannen & Fujita, 2014; Patil & Metri, 2017; Srivastava & Kulkarni, 2017; Guzman Iturra et al., 2018; Chen et al., 2019; Ouchen et al., 2019; Ullah et al., 2019).

There are two main types of SAPF control strategies depending on the current detection point. The first is a load current detection type which is considered an open-loop system in control theory (feedforward control). The second is a closed-loop (feedback control) system in which either the source current or the voltage is measured at the point of common coupling (PCC). Open-loop control systems are very popular and are commonly used in industrial applications because they provide structural stability and do not have the same high computational requirements as feedback control. On the other hand, closed-loop systems provide much higher compensation effectiveness and are characterized by great system robustness against mismatches between control object parameters, as well as insensitivity to nonlinearities caused by dead times and IGBT and diode voltage drops. Schematic diagrams of both types of SAPF controls are shown in Figure 1.

The tasks performed by SAPFs include:

- Source current harmonics compensation;

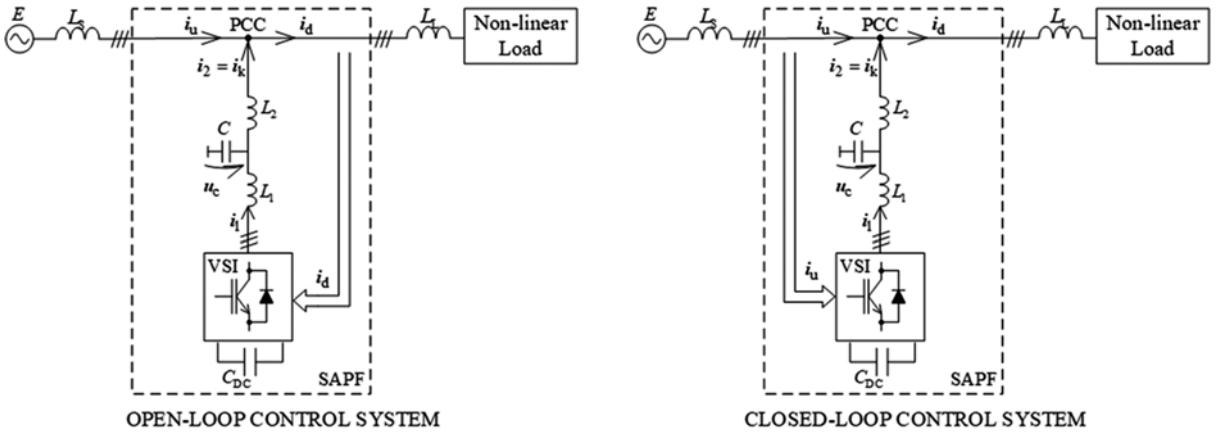

Figure 1. SAPF control in open-loop and closed-loop systems

- Reactive power compensation (compensation of a reactive component of the current fundamental harmonic);
- Unbalanced load current compensation (compensation of current fundamental harmonic negative sequence component).

In this paper, simulations were performed in order to assess the quality of the abovementioned tasks performed in a closed-loop control system and to compare it with an open-loop system.

Control system

The proposed control system is a predictive SAPF control method that allows harmonic currents, reactive power, and unbalanced load current compensation in both a novel closed-loop system and an open-loop system (Wojciechowski, 2012). The block diagram of the control system is shown in Figure 2.

The control algorithm was developed in an orthogonal, stationary reference frame projected on the complex plane α–jβ using the Clarke transformation with power invariance. The zero component was neglected because the SAPF operates in a 3-wire supply system:

$$\begin{bmatrix} i_\alpha & i_\beta \end{bmatrix}^{\mathrm{T}} = \boldsymbol{M} \begin{bmatrix} i_A & i_B & i_C \end{bmatrix}^{\mathrm{T}}$$
$$\begin{bmatrix} u_\alpha & u_\beta \end{bmatrix}^{\mathrm{T}} = \boldsymbol{M} \begin{bmatrix} u_A & u_B & u_C \end{bmatrix}^{\mathrm{T}} \quad (1)$$

where:

$$\boldsymbol{M} = \sqrt{\frac{2}{3}} \cdot \begin{bmatrix} 1 & -\frac{1}{2} & -\frac{1}{2} \\ 0 & \frac{\sqrt{3}}{2} & -\frac{\sqrt{3}}{2} \end{bmatrix}$$

A prediction was applied in the control system because it significantly improved the compensation quality of the SAPF. This required the use of

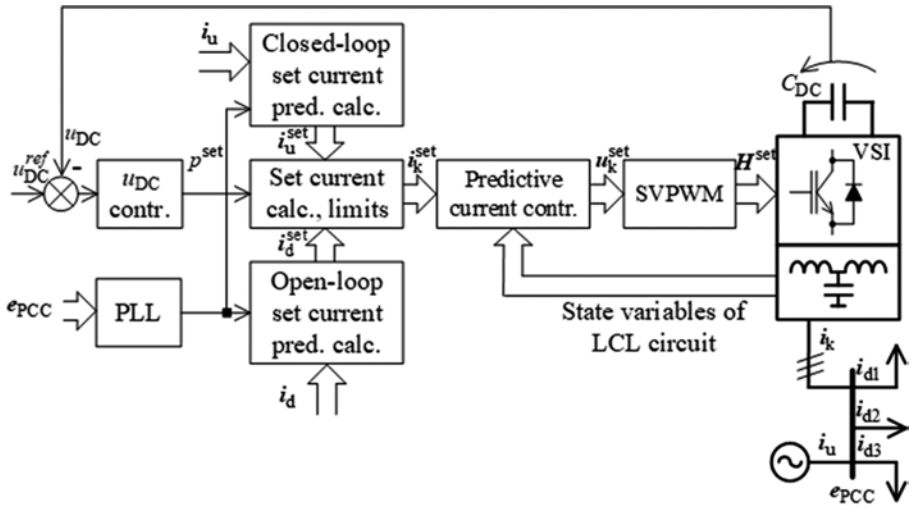

Figure 2. Block diagram of the proposed control system

a predictive current controller to correct for delays between feedbacks and the control. The authorial predictive current controller (Wojciechowski, 2012) implemented in the control system is described by the discrete transfer functions matrix as follows:

$$G_{\mathrm{C}}(z)=\begin{bmatrix} G_{\mathrm{c},i_1\to u(z)} \\ G_{\mathrm{c},i_2\to u(z)} \\ G_{\mathrm{c},u_c\to u(z)} \end{bmatrix}=$$

$$=\begin{bmatrix} \dfrac{-3L_1^2L_2C^2+\left(L_1^2C+4L_1L_2C\right)T_s^2-\left(L_1+L_2\right)T_s^4}{2L_1L_2C^2T_s-L_2CT_s^3+C^2L_1L_2T_s\cdot z} \\ \dfrac{2L_1^2L_2C^2-\left(L_1^2C+4L_1L_2C\right)T_s^2+\left(L_1+L_2\right)T_s^4}{2L_1L_2C^2T_s-L_2CT_s^3+C^2L_1L_2T_s\cdot z} \\ \dfrac{L_1^2L_2C^2-\left(CL_1^2C+3L_1L_2C\right)T_s^2+\left(L_1+L_2\right)T_s^4}{\left(L_2T_s^4-2CL_1L_2T_s^2\right)z-CL_1L_2T_s^2\cdot z^2} \end{bmatrix} \tag{2}$$

where L_1, L_2, and C are consistent with symbols used in Figure 1, and T_s is the sampling period.

The use of predictive current regulation in the control system requires predicting the supply voltage and the designated reference current. The final reference current consists of, depending on the selected SAPF operating variant, the current vector determined in the open-loop or closed-loop systems.

Feedforward control

Predictive harmonics detection is broadband in the presented feedforward method. The set current components used to compensate for the harmonics, reactive power, and unbalanced load current were determined in the time-domain based on Akagi's instantaneous power theory.

The prediction of the set current was based on a cyclic buffer. Assuming that the frequency of the supply voltage remains unchanged, it is possible to presume a constant length of the cyclic buffer l resulting from the quotient of the supply voltage period T_e and the sampling period T_s (Wojciechowski, 2012).

Feedback control

Extraction and prediction of selected harmonic currents in the feedback method is performed in the frequency domain using discrete Fourier transformation (DFT) in accordance with:

$$\underline{I}_{\mathrm{u}}[n]=\frac{1}{K}\sum_{k=0}^{K-1}\underline{i}_{\mathrm{u}}[k]\,\mathrm{e}^{-\frac{\mathrm{j}2\pi nk}{K}} \tag{3}$$

where n is the harmonic order, k is the sample number, and K is the number of samples.

The amplitudes of the individual harmonics of the set current were determined using proportional-integral control. Then, an inverse discrete Fourier transformation (IDFT) was conducted according to the equation:

$$\underline{i}_{\mathrm{u}}[k]=\sum_{k=0}^{N-1}\underline{I}_{\mathrm{u}}[n]\,\mathrm{e}^{\frac{\mathrm{j}2\pi nk}{K}} \tag{4}$$

The prediction involves changing the phases of individual harmonics by a value resulting from the harmonic order n and the prediction horizon r, according to:

$$\Delta\varphi_{\mathrm{n,e,pred}}=n\cdot r\cdot\Delta\varphi_{1,\mathrm{e}} \tag{5}$$

where $\Delta\varphi_{1,\mathrm{e}}$ is the increase in the angle of the fundamental harmonic during one sample period T_s.

The set current vector was obtained by the superposition of acquired individual harmonics:

$$\underline{i}_k^{set}(k+l)=\sum_m \underline{i}_{\mathrm{u},m}(k+l) \tag{6}$$

The block diagram for determining one selected harmonic is shown in Figure 3.

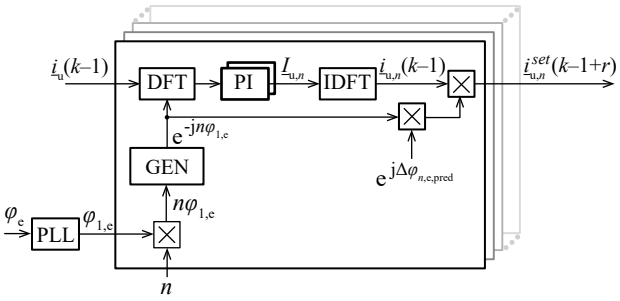

Figure 3. The block diagram of extracting and predicting one current harmonic

The control algorithm ensures the compensation of sixteen current harmonics (both positive and negative) up to the 50th harmonic. Thus, there are 32 algorithms and 64 PI controllers.

Reactive power compensation

The current fundamental harmonic (as well as harmonics that are to be compensated) were designated by utilizing the information about the actual angle of grid voltage, which was determined using a phase-locked loop (PLL). Therefore, the active component of the fundamental harmonic current coincides with

the vector of the fundamental grid voltage harmonics, whereas the reactive component was shifted by 90 degrees. This means that the reactive component of the fundamental current harmonic was the imaginary part of this harmonic on the complex plane. Due to this, the reactive power compensation was based on the compensation of the imaginary part of the current fundamental harmonic positive sequence component that is shown in Figure 4.

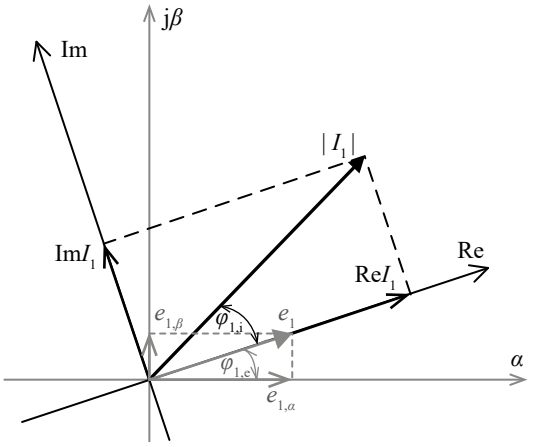

Figure 4. Ideological performance of grid voltage and current fundamental harmonic orthogonal components on the complex plane

The value of reactive power is expressed by:

$$Q_1 = E_1 \cdot I_1 \cdot \sin \varphi_{1,i} = E_1 \cdot \mathrm{Im}\, I_1 \tag{7}$$

Unbalanced load current compensation

The unbalance of a load current is defined, according to the symmetrical components method, as the ratio between the negative sequence component and positive sequence component of a current fundamental harmonic. It is expressed by the following equation:

$$K_{2I} = \frac{I_{-1}}{I_1} \cdot 100\% \tag{8}$$

The value at which K_{2I} equals zero is equivalent to a lack of asymmetry. The magnitude of the current fundamental harmonic negative sequence component is closely related to the value of the K_{2I} coefficient. Therefore, the negative sequence component of a current fundamental harmonic must be compensated for in order to obtain a balanced load current.

Simulation results

Simulations were performed in PLECS by implementing a control algorithm written in C++ programming language. The selected parameters of the tested system are listed in Table 1. Simulations were conducted for both open-loop and closed-loop control systems. The compensation quality of harmonics contained in the source current and voltage were assessed based on the value of total harmonic distortion (THD) coefficient, according to:

$$\mathrm{THD_u} = \frac{\sqrt{\sum_{n=2}^{50} U_n^2}}{U_1}, \quad \mathrm{THD_i} = \frac{\sqrt{\sum_{n=2}^{50} I_n^2}}{I_1} \tag{9}$$

Table 1. Parameters of electrical circuits and control system used in the simulation

Quantity	Value
Line-to-line grid voltage	3×400 V
Line voltage frequency	50 Hz
LCL circuit – L_1	150 µH
LCL circuit – L_2	75 µH
LCL circuit – C	100 µF
Active filter rated power	120 kVA
PWM carrier frequency	8 kHz
Sampling frequency	16 kHz
Nonlinear receiver	6-pulse diode bridge with *RL* load (0,7 Ω, 1 mH)
Deadtime (uncompensated)	3 µs
IGBT voltage drop (uncompensated)	1.5 V
Diode voltage drop (uncompensated)	1.0 V
Grid inductance – L_S	20 µH
Network inductance – L_L	40 µH

Figure 5 presents the grid voltage (E_a, E_b, E_c) and current (I_{ua}, I_{ub}, I_{uc}) waveforms when the compensation is off. Figures 6 and 7 show the current harmonics compensation in open-loop and closed-loop control systems, respectively. In addition to the waveforms of voltages and currents in PCC, the figure also depicts waveforms of the phase currents of inductors L_1 (I_{1a}, I_{1b}, I_{1c}) and L_2 (I_{2a}, I_{2b}, I_{2c}).

The $\mathrm{THD_u}$ coefficient decreased by more than 6.5 times after compensation in the open-loop system and by almost 16.5 times after compensation in the closed-loop control system, which is a difference of almost 2.5. Moreover, the $\mathrm{THD_i}$ value was 4 times smaller in the feedback control method than in the feedforward method, which confirms the superior current harmonics compensation quality in the closed-loop control system.

Figures 8 to 11 concern the reactive power compensation. Figure 8 presents the waveform of reactive power in the PCC of the open-loop system, while Figure 9 shows the waveform of the

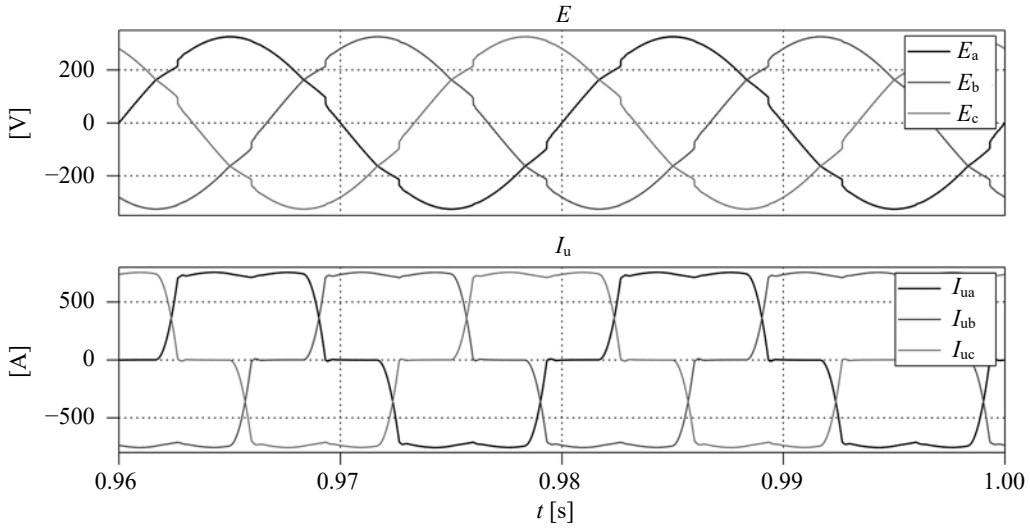

Figure 5. System operation without harmonics compensation; THD_u = 2.8%, THD_i = 24%

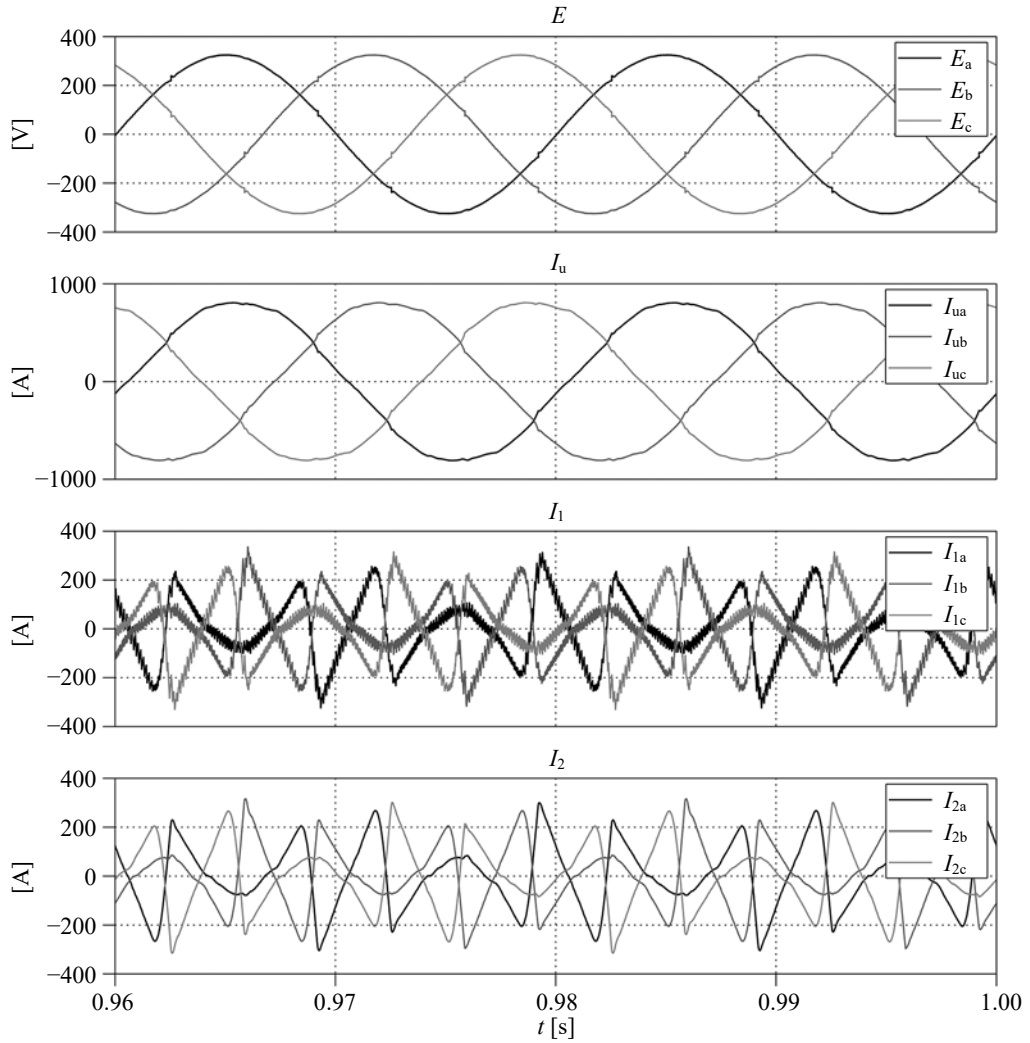

Figure 6. Open-loop broadband current harmonics compensation; THD_u = 0.42%, THD_i = 3.17%

value of the current fundamental harmonic reactive component in the open-loop control system. Figures 10 and 11 depict the respective waveforms in the closed-loop control system. The turning time on the reactive power compensation was 0.5 s in all cases.

The absolute value of reactive power decreased about seven times after compensation in the

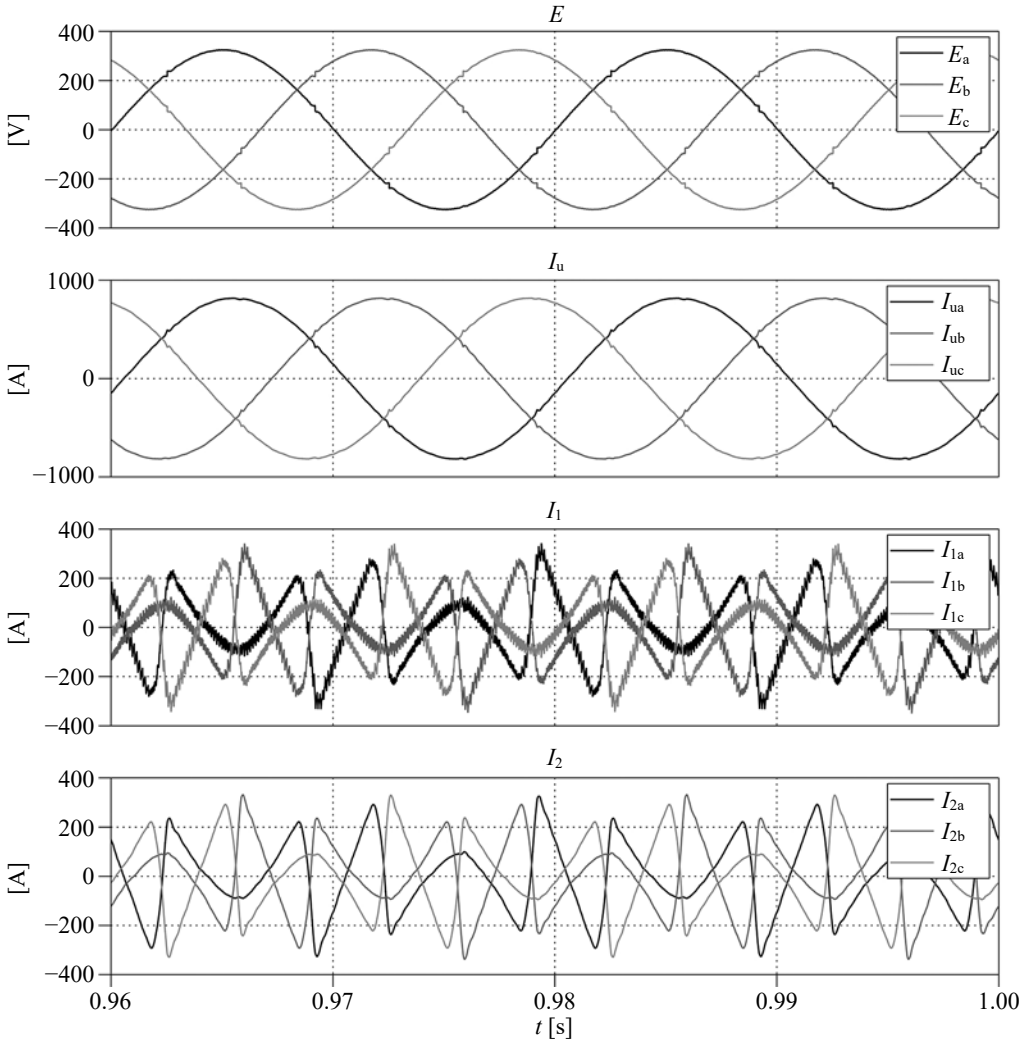

Figure 7. Closed-loop selective current harmonics compensation; THD_u = 0.17%, THD_i = 0.72%

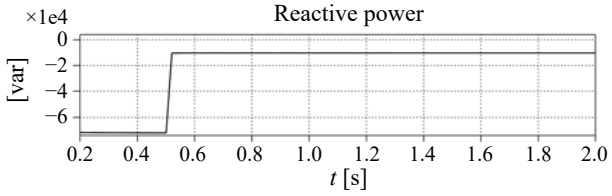

Figure 8. Open-loop system; Q_1 = –72,012 var before compensation; Q_1 = –10,219 var after compensation

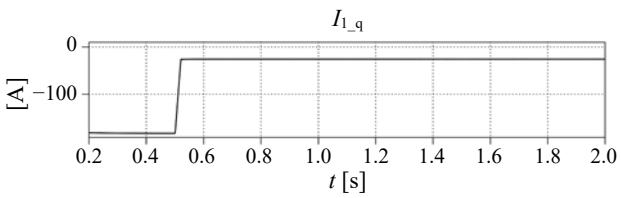

Figure 9. Open-loop system; ImI_1 = –181.2 A before compensation; ImI_1 = –25.7 A after compensation

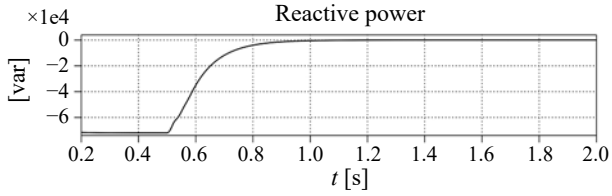

Figure 10. Closed-loop system; Q_1 = –72,012 var before compensation; Q_1 = –0.008 var after compensation

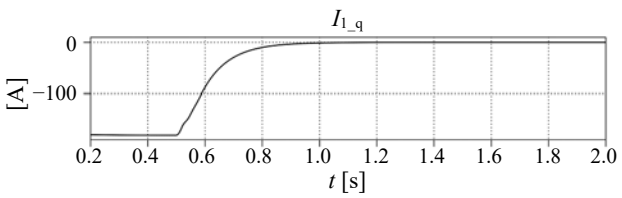

Figure 11. Closed-loop system; ImI_1 = –181.2 A before compensation; ImI_1 = –0.00002 A after compensation

open-loop system, and the current fundamental harmonic reactive component increased by –25.7 A. However, this component was near zero in the closed-loop control system which is reflected in the total compensation of the reactive power.

To simulate an unbalanced load current, the inductance of one network inductor was changed from 40 μH to 140 μH. Figure 12 presents the results of an unbalanced load current compensation in an open-loop system, while the results obtained for a closed-loop system are depicted in Figure 13. Both figures consist of two waveforms and show the state before and after compensation with a turning time during compensation of 0.5 s. The first depicts the waveform magnitude of the current fundamental harmonic negative sequence component, and the second depicts the waveform of the K_{2I} coefficient.

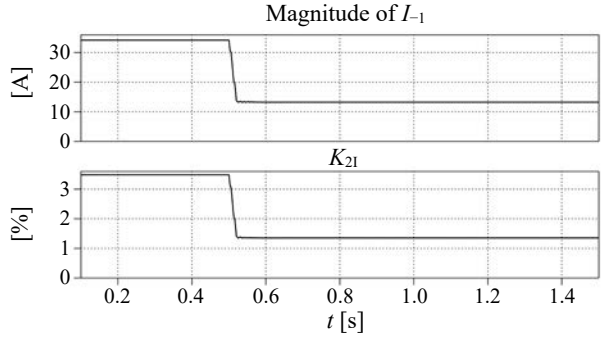

Figure 12. Open-loop system; $|I_{-1}|$ = 34.2 A, K_{2I} = 3.49% before compensation; $|I_{-1}|$ = 13.25 A, K_{2I} = 1.35% after compensation

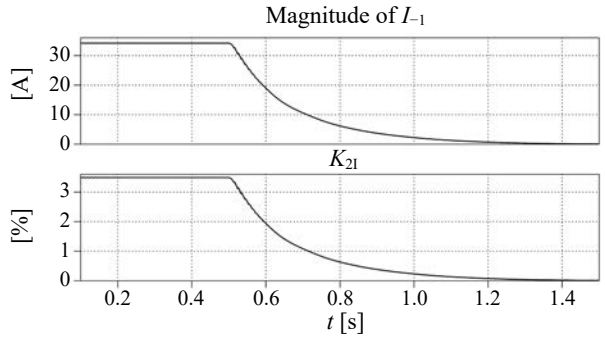

Figure 13. Closed-loop system; $|I_{-1}|$ = 34.2 A, K_{2I} = 3.49% before compensation; $|I_{-1}|$ = 0.092 A, K_{2I} = 0.009% after compensation

The magnitude of the current fundamental harmonic negative sequence component and the value of the K_{2I} coefficient decreased by more than 2.5 times after compensation in the open-loop control system. In the closed-loop control system, the unbalanced load current was almost completely compensated for, and the value of the K_{2I} coefficient reached 0.009%.

Conclusions

The presented control system enables the predictive control of SAPFs in both open-loop and closed-loop systems. The simulation results showed that the compensation quality in a closed-loop control system was greater than in an open-loop system. This was observed in all three tasks performed by the SAPF in this paper, including harmonic currents, reactive power, and unbalanced load current compensation. The supply current THD_i coefficient obtained using the feedback method was less than 1%, while it was above 3% using the feedforward method. The absolute value of the reactive power was compensated to 10,219 var from 72,012 var in the open-loop system, while in the closed-loop control system, it was fully compensated. The unbalance in the load current, expressed by the K_{2I} coefficient, was compensated from 3.49% to 1.35% in the feedforward method. However, in the feedback control method, it gained almost 0%. Further research is planned to conduct experimental tests in order to assess the feasibility of using this control algorithm in active power filters for industrial solutions.

References

1. Asiminoaeiand, L., Cristian, L., Blaabjerg, F. & Boldea, I. (2006) *Harmonic Mitigation Improvement with a New Parallel Topology for Shunt Active Power Filters*. 37th IEEE Power Electronics Specialists Conference.
2. Chen, W., Zhang, D., Zhang, H., Wang, Z. & Sun, M. (2019) *The Research on Composite Control Strategy of Active Power Filter*. 2019 34th Youth Academic Annual Conference of Chinese Association of Automation (YAC).
3. Guzman Iturra, R., Cruse, M., Mütze, K., Dresel, C., Soleimani, I. & Thiemann, P. (2018) *Model Predictive Control for Shunt Active Power Filter with Harmonic Power Recycling Capability*. 2018 International Conference on Smart Energy Systems and Technologies (SEST).
4. Mannen, T. & Fujita, H. (2014) Shunt Active Power Filter Based on Source Current Detection With Fast Transient Response. *IEEE Energy Conversion Congress and Exposition (ECCE).*
5. Mariethoz, S. & Rufer, A.C. (2002) Open Loop and Closed Loop Spectral Frequency Active Filtering. *IEEE Transactions on Power Electronics* 17, 4, pp. 564–573.
6. Mattavelli, P. (2001) A Closed-loop Selective Harmonic Compensation for Active Filters. *IEEE Transaction on Industry Applications* 37 (1), pp. 81–89.
7. Mattavelli, P. & Marafão, F.P. (2004) Repetitive-Based Control for Selective Harmonic Compensation in Active Power Filters. *IEEE Transactions on Industrial Electronics* 51, 5, pp. 1018–1024.
8. Ouchen, S., Steinhart, H., Blaabjerg, F., Benbouzid, M., Betka, A. & Gaubert, J.P. (2019) *Performance Analysis of Direct Power Control with Space Vector Modulation for Shunt Active Power Filter*. IECON 2019 – 45th Annual Conference of the IEEE Industrial Electronics Society.

9. Patil, S. & Metri, R.A. (2017) Power quality improvement using shunt active power filter. *IEEE International Conference on Data Management, Analytics and Innovation (ICDMAI)*.
10. Srivastava, G.D. & Kulkarni, R.D. (2017) *Design, simulation and analysis of shunt active power filter using instantaneous reactive power topology*. Proc. of IEEE Int. Conf. on Nascent Technologies in Engineering (ICNTE) – Conf. proc. pub. in IEEE Xplore Digital Library.
11. Ullah, A., Sheikh, I.U.H., Arshad, S. & Saleem, F. (2019) *Digital Active Power Filter Controller Design for Current Harmonics in Power System*. 16th International Bhurban Conference on Applied Sciences and Technology (IBCAST) 2019, pp. 384–388.
12. Wojciechowski, D. (2012) Unified LCL circuit for modular active power filter. *COMPEL – The international journal for computation and mathematics in electrical and electronic engineering* 31, 6, pp. 1985–1997.